The Astrophysical Journal, 568:312–323, 2002 March 20

OUTFLOW-INDUCED DYNAMICAL AND RADIATIVE INSTABILITY IN STELLAR ENVELOPES WITH AN APPLICATION TO LUMINOUS BLUE VARIABLES AND WOLF-RAYET STARS

Richard B. Stothers
Institute for Space Studies, NASA Goddard Space Flight Center, 2880 Broadway, New York, NY 10025
Received 2001 June 8; accepted 2001 November 21

ABSTRACT

Theoretical models of the remnants of massive stars in a very hot, post–red-supergiant phase display no obvious instability if standard assumptions are made. However, the brightest observed classical luminous blue variables (LBVs) may well belong to such a phase. A simple time-dependent theory of moving stellar envelopes is developed in order to treat deep hydrodynamical disturbances caused by surface mass loss and to test the moving envelopes for dynamical instability. In the case of steady state outflow, the theory reduces to the equivalent of the Castor, Abbott, & Klein formulation for optically thick winds at distances well above the sonic point. The time-dependent version indicates that the brightest and hottest LBVs are both dynamically and radiatively unstable, as a result of the substantial lowering of the generalized Eddington luminosity limit by the mass-loss acceleration. It is suggested that dynamical instability, by triggering secular cycles of mass loss, is primarily what differentiates LBVs from the purely radiatively unstable Wolf-Rayet stars. Furthermore, when accurate main-sequence mass-loss rates are used to calculate the evolutionary tracks, the predicted surface hydrogen and nitrogen abundances of the blue remnants agree much better with observations of the brightest LBVs than before.

Subject headings: stars: evolution — stars: mass loss — stars: oscillations — stars: variables: other — stars: Wolf-Rayet

1. INTRODUCTION

The evolutionary status of the luminous blue variables (LBVs or S Doradus variables) and the underlying cause of their large cyclical outbursts are still under intense debate. At least for the fainter and cooler LBVs, an abundance of evidence now suggests that these are post–red-supergiant stars (van Genderen 2001; de Jager et al. 2001), just as Lamers, de Groot, & Cassatella (1983) originally proposed from their observed locations on the Hertzsprung-Russell (H-R) diagram. Since modern theoretical evolutionary tracks can account very well for the detailed characteristics of these cooler LBVs, especially if the stars are dynamically unstable as a result of high radiation pressure and partial ionization of hydrogen and helium in their outer envelopes (Stothers & Chin 1996; Stothers 1999c), it is reasonable to try to apply the same type of post–red-supergiant explanation to the brighter and hotter LBVs as well. On the other hand, it is also possible to see these hotter objects as main-sequence stars, which are experiencing pulsationally or rotationally enhanced mass loss following widespread interior mixing—perhaps mixing by rotational currents since many upper main-sequence stars are observed to be fast rotators (Langer et al. 1994; Pasquali et al. 1997; Lamers et al. 2001).

In practice, serious problems bedevil both the main-sequence and post–red-supergiant explanations for the brightest LBVs. The main-sequence hypothesis suffers a possible problem with the very small mass, 23 $M_{\odot}$, measured for P Cyg from an atmospheric analysis (Pauldrach & Puls 1990). Furthermore, the near uniformity of the observed LBV surface hydrogen abundances, as well as their specific values of $X_{\rm surf} = 0.3$–0.4, can be accounted for only in a very ad hoc way. Plausible assumptions must be made for the probability of very fast rotation, the rotational mixing time, the degree of ineffectiveness of the mean molecular weight barrier, the instability mechanism, the rate of enhanced mass loss, and the cause of the mass loss cyclicity. Regarding possible mechanisms, radial strange-mode pulsations are now believed to produce only the observed *micro-variations* in LBVs (van Genderen 2001), while the existence of rotational instability near the Eddington luminosity limit (Langer 1997) depends on how the Eddington limit is defined in the presence of rotation (Glatzel 1998; Stothers 1999b; Baumgarte & Shapiro 1999; Maeder 1999; Maeder & Meynet 2000b). According to one interpretation, Maeder & Meynet (2000b) have argued that if the rotational velocity approaches break-up, enormous mass-loss rates might occur for stars with $\log (L/L_{\odot}) > 5.8$ (the luminosity limit of known red supergiants) and at $T_e < 30{,}000$ K (the effective temperature limit of known LBVs).

Gas nebulae ejected from four LBVs show N/O abundance ratios that indicate a mixture of original stellar gas and CNO-processed material but are otherwise rather complicated to interpret (Smith et al. 1998; Lamers et al. 2001). In the case of the nebulae around R127 and S119, the very low expansion velocities and the long kinematical ages may indicate a red supergiant, rather than a main-sequence, ejection event (Smith et al. 1998). The larger expansion velocity of 70 km s^{-1} exhibited by the AG Car nebula suggests a yellow hypergiant origin (Robberto et al. 1993; Smith et al. 1997; de Jager 1998; Stothers & Chin 1999), which could account for the presence of dust in the nebula (Voors et al. 2000). As for the P Cyg nebula, its high expansion velocity, short kinematical age, and tiny mass all point to a very recent (LBV) origin; however, there is some evidence for a more distant and older nebula, which could imply a red-supergiant event 10^4–10^5 yr ago (Meaburn et al. 2000). Although in all these cases it remains possible to imagine a temporary pseudo–red-supergiant state which might develop after an enormous main-sequence outburst (Smith

et al. 1998; Lamers et al. 2001), the known outbursts of LBVs have always led to effective temperatures that are no cooler than ~8000 K (Humphreys & Davidson 1994). Moreover, bipolar structure seen in some of the LBV nebulae does not necessarily indicate rapid rotation of an underlying main-sequence star, because such structure appears even in the nebulae around very luminous yellow and red supergiants like IRC +10420 (Nedoluha & Bowers 1992; Oudmaijer et al. 1996; Humphreys et al. 1997) and VY CMa (Wittkowski, Langer, & Weigelt 1998).

Turning now to the existing difficulties with the post–red-supergiant hypothesis for the brightest LBVs, they are as follows: No red or yellow supergiants are known brighter than $\log (L/L_{\odot}) \approx 5.8$ (Humphreys & Davidson 1979; de Jager 1998). This may not be a serious obstacle, despite appearances, because the predicted lifetime in the yellow-red region is only several 10^4 yr, at most (Stothers & Chin 1999). Predicted surface hydrogen abundances, however, are definitely too low, $X_{\rm surf} = 0.1$–0.2 (Stothers & Chin 2000). Related to this discrepancy is a potential surface nitrogen problem (Lamers et al. 2001). Moreover, it is still not possible to predict the rate of enhanced mass loss due to dynamical instability, which, along with the rate of stellar-wind mass loss for red supergiants, remains the primary unconstrained parameter. Finally, the observed hot LBV effective temperatures of 20,000–30,000 K fail to be matched by the theoretically predicted values of 10,000–16,000 K. To save the post–red-supergiant hypothesis, it is necessary to assume that the brightest LBVs are evolving along transient blue loops that emerge from the yellow and red supergiant region as a result of dynamical instability (Stothers & Chin 1999). This possibility, however, does not explain why observed LBV outbursts develop in the blue region itself and why LBVs at quiescence dwell only in this region.

The present paper addresses in detail these persistent shortcomings of the post–red-supergiant hypothesis. It will be shown that they arise from our oversimplified assumptions about the magnitude of the stellar wind and the effect of the wind on the underlying envelope. Revised stellar models for the brightest LBVs achieve nearly the observed surface hydrogen (and nitrogen) abundances and successfully reach dynamical instability at very hot effective temperatures. Still hotter models develop radiative instability, which may also explain the high mass-loss rates of the Wolf-Rayet stars, as Kato & Iben (1992) originally suggested.

In § 2, the main physical ingredients of our new stellar models are described, including the atomic opacities, treatment of convection, and rates of stellar-wind mass loss on and off the main sequence. Our revised surface hydrogen (and nitrogen) abundances for the brightest LBVs are derived and discussed in § 2.3.1. The problem of excessively low effective temperatures of our earlier LBV models is addressed in § 3 by means of an extensive parameter study, examining all of the standard free parameters. Since nothing obvious seems to work, we next examine, in §§ 4 and 5, the possible effect of the acceleration of mass loss on the structure and stability of the stellar envelope. Showing great potential, this factor is then incorporated into revised stellar models in § 6, and leads to our final, successful results. In § 7 a self-contained overview of our current theoretical picture of LBVs and of their close relatives, the hydrogen-poor WN stars, is presented.

2. PHYSICAL ASSUMPTIONS

2.1. *Opacities*

OPAL opacities (Rogers & Iglesias 1992; Iglesias, Rogers, & Wilson 1992), which are generally very close to the OP opacities of Seaton et al. (1994), continue to be used in our stellar models. Published updates (Iglesias & Rogers 1996) have led to no radical revision of the opacities, although the new values are ~20% larger in the iron opacity bump region around $T = 2 \times 10^5$ K, chiefly because of the inclusion of additional metals in the mixture. Since the relevant layers in massive stars are already strongly convective, the structure of these layers is not expected to be changed appreciably. Nevertheless, we have conducted one test using the opacity updates. The original OPAL opacities have been artificially modified by multiplying them by a triangular function,

$$p = \max (1.0, p_{\max} - 0.5|\log T - 5.3|) . \quad (1)$$

When these revised opacities are employed with $p_{\max} = 1.2$ in an evolutionary rerun for an initial stellar mass of 60 $M_{\odot}$, hardly any change takes place (§ 3).

2.2. *Convection*

To determine the point of outbreak of convection as well as the extent of the mixing of material in convective and semiconvective layers, we have adopted the Schwarzschild (temperature-gradient) criterion as being approximately correct for stars of very high mass (Stothers & Chin 2000). We have everywhere set to zero the distance of convective overshooting beyond the formal Schwarzschild boundary.

In the superadiabatic layers near the stellar surface, standard mixing-length theory has been used, with a ratio of mixing length to local pressure scale height, α_p, set to either 1.4 or 2.8 (Stothers & Chin 1997). Because of the physical separateness of the multiple convection zones formed by the partial ionizations of hydrogen, helium, and the iron group of elements in hot stars, a more sophisticated theory of convection would be unwarranted at present.

Turbulent pressure in all of these convection zones has been ignored, although mixing-length theory predicts the attainment of supersonic velocities in the iron convection zone in the hottest and most luminous stellar models. Since the iron convection zone always lies at the base of the outer envelope, turbulent pressure would probably not contribute very much to the integral condition governing dynamical stability (§ 4).

2.3. *Rates of Stellar-Wind Mass Loss*

2.3.1. *Main-Sequence Mass-Loss Rates and Their Consequences*

For O-type stars, the standard rates of stellar-wind mass loss in the convenient form of a fitted formula published by Nieuwenhuijzen & de Jager (1990) have been used here, as they seem to be confirmed by the recent observations of Lamers et al. (1999):

$$-\frac{dM}{dt} = 1.17 \times 10^{-8} \left(\frac{L}{L_{\odot}}\right)^{1.64} \left(\frac{M}{M_{\odot}}\right)^{0.16} T_e^{-1.61} . \quad (2)$$

The units of the mass-loss rate here and throughout this paper are $M_{\odot}$ yr^{-1}.

During the course of the main-sequence phase, very massive stars evolve from type O to type B. Unfortunately, mass-loss rates for the most luminous B-type supergiants

are overestimated by equation (2), judging from the improved rates for O and B supergiants that have been published by Scuderi et al. (1998). Since agreement with Lamers et al. (1999) is excellent for the O-type supergiants, the following rates from Scuderi et al. will be applied whenever the rates predicted by equation (2) exceed them:

$$-\frac{dM}{dt} = 2.5 \times 10^{-13} \left(\frac{L}{L_\odot} \right)^{1.25} . \quad (3)$$

In practice, the overestimation of the amount of mass loss caused by using equation (2) hardly affects the evolutionary tracks for initial masses $M \leq 60\ M_\odot$, but in one important respect it does alter the evolution at higher masses—by lowering the predicted surface hydrogen abundance, $X_{\rm surf}$, during the LBV phase. The basic reason for the lowering of $X_{\rm surf}$ is that excessively heavy mass loss on the main sequence weakens convective instability in the inner envelope; as a consequence, the fully convective zone (FCZ) that later develops just above the hydrogen-burning shell has a smaller mass as well as a lower hydrogen content, X_f, than in the absence of mass loss. When further evolution with mass loss eventually exposes the FCZ, $X_{\rm surf}$ becomes equal to X_f, which for an initial stellar mass of 90 $M_\odot$ is only 0.11 if equation (2) is adopted. Observations, however, show $X_{\rm surf} = 0.3$–0.4 (see the references and discussion in Stothers & Chin 2000). Since our analogous stellar models for 30–60 $M_\odot$ agree very well with these observed surface hydrogen abundances, the large discrepancy for 90 $M_\odot$ is hard to explain unless the amount of mass loss is less than expected from equation (2).

When the present prescription for main-sequence mass loss based on the use of equation (3) is applied, the models for 90 $M_\odot$ attain $X_{\rm surf} = 0.24$. This represents a remarkable improvement, considering the uncertainty of the predicted size of the FCZ. It should be noted that several earlier attempts to utilize observations of $X_{\rm surf}$ in order to detect the FCZ in a massive star did not produce unambiguous results (Stothers & Chin 1976; Langer 1987; Staritsin & Tutukov 1989).

To derive an estimate of the expected surface nitrogen abundances (which we have not calculated), we use the evolutionary tracks for stars of 25–85 $M_\odot$ by Schaller et al. (1992), who adopted input physics similar to our standard set, and so obtained stellar models very much like ours (Stothers & Chin 2000). Following Lamers et al. (2001), we focus on the number ratio N/O of the nitrogen and oxygen abundances. Our primary assumption is that N/O correlates inversely with X_f in a more or less unique way, regardless of the fact that we are using stellar models with different initial masses rather than stellar models with a fixed initial mass but with different assumed sizes of the FCZ (due to different assumed main-sequence mass-loss rates). Although the tables of Schaller et al. (1992) do not explicitly list X_f, this quantity can be read off from their listed values of surface H after mass loss has exposed the FCZ, while the accompanying surface N and O abundances yield the number ratio N/O. Ideally, we should be using fully self-consistent stellar models in the present study. However, all that we really need from Schaller et al. is their nucleosynthesis data, which in essence comprise a sequence of correlated He, N, and O abundances that should be quite general. We thus find $\log (\mathrm{N/O}) = 2.5 - 4.5 X_f$ for $0.18 \leq X_f \leq 0.46$. The reason for this correlation is that if the FCZ is large, convective mixing penetrates farther outward into the less highly CNO-processed layers of the star. Therefore, rapidly mixed material in the FCZ contains both a higher hydrogen abundance and a lower N/O number ratio than would be the case if the FCZ were smaller.

Since observations of very bright LBVs show $X_f \approx 0.35$, we can predict $\mathrm{N/O} \approx 8$ from the Schaller et al. (1992) models. Photospheric values of N/O are not known for these LBVs, but the surrounding gas nebulae show $\mathrm{N/O} \approx 1$–6 (Lamers et al. 2001). Since the nebulae are expected to consist mostly of ejected FCZ material plus some less evolved material, we would anticipate finding N/O to be somewhat lower than $\sim$8 in the nebulae. The apparent agreement with the post–red-supergiant models containing FCZs is striking, considering that fully CNO-processed material has $\mathrm{N/O} \approx 60$ while unprocessed original material has $\mathrm{N/O} \approx 0.1$. The post–red-supergiant comparison made by Lamers et al. (2001) was unsuccessful, because they did not recognize the significance of the FCZ and they used stellar models that had suffered too much main-sequence mass loss and so contained unrealistically small FCZs (Meynet et al. 1994).

2.3.2. *Red Supergiant Mass-Loss Rates*

Rates of stellar-wind mass loss in the red-supergiant region are very poorly known (Salasnich, Bressan, & Chiosi 1999; Josselin et al. 2000). To be sufficiently conservative, we allow the possibility that for each initial stellar mass the rate of mass loss might be such that the star could leave the red-supergiant branch at any time between the beginning and the end of central helium burning. Accordingly, as soon as the star reaches the red region (taken here to be $\log T_e < 3.7$), we begin to remove mass at an arbitrarily high rate until the star leaves the red region with its central helium abundance, Y_c, still undepleted. The object that emerges after the envelope stripping is the most massive and least evolved blue-remnant model possible for the given initial stellar mass. (This scenario would also apply if Roche lobe overflow in a binary system were to cause the mass loss.) Further evolution of the blue remnant, allowing no additional mass loss, produces a sequence of stellar models with progressively reduced Y_c, each of which in principle could have been reached by adopting a smaller rate of red-supergiant mass loss.

2.3.3. *Post–Red-Supergiant Mass-Loss Rates*

In the blue-remnant phase, rates of mass loss are uncertain enough that we have decided to cover the whole range of physical possibilities, from no mass loss at all to the instantaneous removal of the whole residual hydrogen envelope, which represents the maximum loss possible. Observed rates of mass loss from LBVs and from hydrogen-poor WN stars, although uncertain, can later be used to provide some constraints on the selection of relevant blue-remnant models (§ 6).

Returning to the original blue-remnant model, if a small amount of additional mass is arbitrarily removed and evolution is again allowed to proceed without further mass loss, a parallel sequence of stellar models is obtained. By repeating this process with successively greater amounts of initial mass removed each time, we end up with a two-dimensional grid of stellar models, specified by the two parameters, M

and Y_c. This grid contains all possible blue-remnant models for the given initial main-sequence mass.

3. UNMODIFIED STELLAR EVOLUTIONARY MODELS

To obtain a starting model for the blue-remnant phase, an evolutionary sequence is computed from the zero-age main sequence to the region of red supergiants. Then mass is peeled off very quickly until a blue remnant is formed. Initial stellar masses adopted are 30, 45, 60, and 90 $M_\odot$. For the initial hydrogen and metals abundances by mass we adopt $X_e = 0.70$ and $Z_e = 0.03$. The blue-remnant mass turns out to be roughly equal to $\frac{1}{3}$ of the initial stellar mass.

Once we have acquired a blue-remnant model, a set of parallel evolutionary tracks for the phase of core helium burning is generated at constant mass, as described in § 2.3.3. Each of these evolutionary tracks is identified by the mass of the blue remnant, ranging from the maximum possible mass, when the progenitor has just left the red-supergiant region, down to the minimum possible mass, when the blue remnant has just had its hydrogen envelope completely removed. Accordingly, $X_{\rm surf}$ ranges from X_f to 0. Typical evolutionary tracks on the H-R diagram have already been displayed in several of our recent papers (e.g., Stothers & Chin 1996, 1999). The main point to note here is that the blue remnant immediately takes up a very blue position, which is hotter for a smaller mass remaining in the hydrogen envelope but is typically in the range $\log T_e = 4.6$–4.9. This initial position falls along a "generalized zero-age main sequence" for unevolved helium stars that contain small, homogeneous hydrogen envelopes (Cox & Salpeter 1961; Giannone 1967; Simon & Stothers 1969). Afterward, the blue remnant evolves slowly redward, gradually depleting helium in its core.

Each model along each of the evolutionary tracks is tested for dynamical instability by employing standard linear adiabatic perturbation theory and rigorously computing the eigenvalue (§ 4), but no allowance is made for the possible effect of the mass-loss acceleration on either the equilibrium structure of the stellar model or its dynamical stability or instability. We return to this important question later. Table 1 contains our results for a sample of blue-remnant models in the case of our four adopted initial main-sequence masses of 30, 45, 60, and 90 $M_\odot$. The table begins, in each case, with the maximum possible mass for the blue remnant and continues with progressively reduced masses, until either the hydrogen envelope is completely removed ($X_{\rm surf} = 0$) or the central helium abundance becomes very low ($Y_c = 0.003$) at the specific time when the blue remnant crosses the threshold of dynamical instability. (Dynamical instability occurs when the hydrostatic equilibrium of the envelope is lost.) Since the L/M ratio increases as a result of surface mass loss and of interior chemical evolution, the threshold effective temperature gradually becomes hotter as mass is removed, although it never goes past a relatively moderate value of 17,000 K, which is still too cool to explain the hottest LBVs with effective temperatures as high as 30,000 K.

This raises the question of whether the L/M ratio can somehow be increased further by including several neglected factors. The normal evolutionary rise of the star's luminosity is due to four effects: (1) the thermonuclear conversion of helium into carbon (and then oxygen) near the center, which increases the mean molecular weight of the convective core; (2) the outward growth of the convective core, which means more helium being consumed; (3) the outward march of the hydrogen-burning shell, which adds material of higher mean molecular weight (helium) to the outer core; and (4) the increased power output from both the core and the hydrogen-burning shell, as the star heats up in consequence of fast core contraction toward the end of central helium burning. In the present models, the hydrogen-burning shell is virtually extinct, owing to the very small mass contained within the residual hydrogen envelope. There is some uncertainty, however, about the adopted rate of the $^{12}C(\alpha,\gamma)^{16}O$ reaction, as well as about the adopted distance of convective overshooting beyond the standard Schwarzschild boundary of the convective core. We have increased both factors by arbitrarily large amounts, but have found that the model luminosities change imperceptibly.

How might axial rotation of the star affect our conclusions? Many upper main-sequence stars are observed to be rapid rotators. These objects might conceivably follow very different evolutionary paths than nonrotators do (Maeder & Meynet 2000a; Lamers et al. 2001). Fortunately for our purposes, the prior history of the blue remnant is relatively unimportant in the context of the present models, since it would have been sufficient for us to have assigned the

TABLE 1

THRESHOLD OF DYNAMICAL INSTABILITY FOR UNMODIFIED MODELS IN THE CASE $\alpha_P = 1.4$

Initial $M/M_\odot$	Remnant $M/M_\odot$	Envelope $\Delta M/M_\odot$	$X_{\rm surf}$	$\log(L/L_\odot)$	Y_c	$\log T_e$
30.....	10.4	0.3	0.22	5.474	0.003	4.03
45.....	15.4	0.8	0.39	5.572	0.19	3.79
	14.9	0.3	0.39	5.592	0.09	3.91
	14.8	0.2	0.36	5.613	0.02	4.01
	14.8	0.2	0.24	5.657	0.003	4.11
60.....	21.6	1.1	0.27	5.802	0.24	3.97
	20.9	0.4	0.24	5.811	0.14	4.06
	20.8	0.3	0.16	5.841	0.03	4.13
	20.7	0.2	0.09	5.877	0.003	4.20
90.....	34.6	0.8	0.24	6.052	0.95	4.07
	34.4	0.6	0.23	6.057	0.82	4.10
	34.3	0.5	0.07	6.113	0.22	4.16
	34.0	0.2	0.03	6.125	0.08	4.18
	32.0	0.0	0.00	6.119	0.02	4.24

TABLE 2
THRESHOLD OF DYNAMICAL INSTABILITY FOR UNMODIFIED MODELS WITH CHANGED INPUT PARAMETERS

$p_{\max}$	α_P	$\log(L/L_\odot)$	Y_c	$\log T_e$
1.0.....	1.4	5.841	0.03	4.13
1.2.....	1.4	5.825	0.06	4.10
1.0.....	2.8	5.880	0.003	4.18

NOTE.—Remnant $M/M_\odot = 20.8$, Envelope $\Delta M/M_\odot = 0.3$, $X_{\rm surf} = 0.16$.

helium core mass and the hydrogen envelope mass without reference to the star's previous evolution. The angular momentum stored in the core, however, could be significant (Heger & Langer 1998). A previous study of the possible effect of angular momentum on the dynamical stability of blue-remnant models has demonstrated that the change of the star's L/M ratio due to fast core rotation is the most important factor (Stothers 1999b). If the blue remnant's mass is assigned, however, the change in luminosity is expected to be very small compared to the evolutionary changes caused by the depletion of helium. Assuming approximately rigid rotation in the core (Endal & Sofia 1978), we have found that rotating models of massive helium cores, constructed by solving the rotational equations of Sackmann & Anand (1970), yield a drop in luminosity that is only $\delta \log(L/L_\odot) = -0.02$ even for the extreme case of equatorial breakup velocity.

Some of the input physics used for the outer envelope, like that used for the core, is imperfectly known. If the star's evolution were frozen in time, an increase of opacity or a decrease of the convective mixing length would raise the local ratio of radiation pressure to total pressure, and so would tend to shift the star in the direction of dynamical instability. On the other hand, the evolving structure of the envelope must adjust as a whole to any change of the input physics. If the relative amount of radiation pressure increases, the envelope will expand faster and so will arrive at the threshold of dynamical instability at an earlier stage of central helium depletion, and therefore at a lower luminosity. The stabilizing effect of a lower luminosity at least partially counters the destabilizing effect of a higher radiation pressure. As a result, the effective temperature of a star that has reached the threshold of dynamical instability does not necessarily increase when an ostensibly destabilizing change is made in one of the input parameters. Table 2 shows, in fact, that a change in either $p_{\max}$ or α_p (§ 2) leads to a virtual cancellation of the stabilizing and destabilizing effects.

How all these results play out on the H-R diagram can be seen in Figure 1. Each plotted locus refers to one of our four adopted initial main-sequence masses. Redward of the four loci lies the predicted domain of dynamical instability.

Empirical values of luminosity and effective temperature for actual LBVs and LBV candidates that belong to the Galaxy and the Large Magellanic Cloud have been tabulated by van Genderen (2001). We adopt van Genderen's values here, but omit six objects listed by him as having uncertain luminosities and also five outlying objects having $\log(L/L_\odot) < 5.25$, which appear excessively faint. Very bright LBVs with $\log(L/L_\odot) > 6.3$ are not considered in this paper. Following Sterken, de Groot, & van Genderen (1997), we tentatively regard ζ^1 Sco as an uncertain LBV and therefore omit it. This leaves us with 20 stars, which are plotted as asterisks in Figure 1.

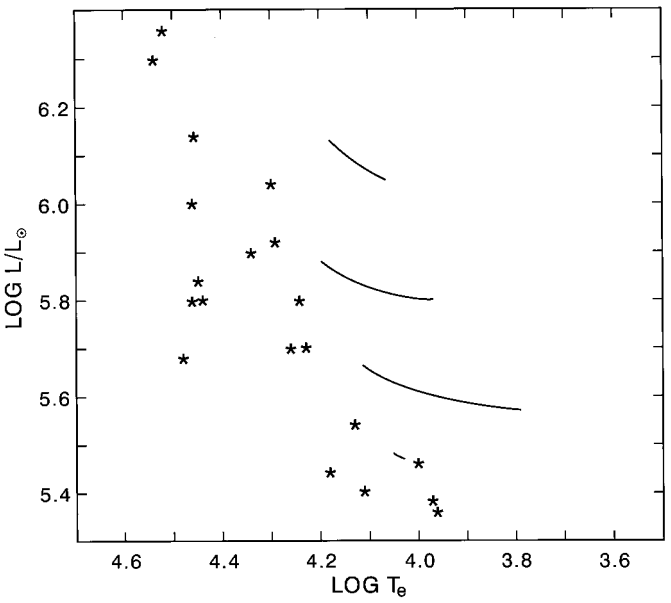

FIG. 1.—H-R diagram showing the possible locations of stellar models at the onset of the blue phase of dynamical instability, for four blue-remnant masses in the case $\alpha_P = 1.4$. None of the models contains any allowance for the effect of the mass-loss acceleration. To the right of the loci lies the domain of dynamical instability. Asterisks denote observed LBVs and LBV candidates at quiescence.

Notice that, within the possible errors of measurement, the six faintest stars have locations that agree very well with our theoretical predictions for dynamically unstable blue-remnant models. At brighter luminosities, however, the models are definitely too cool. This disagreement has been a problem since our original discovery of the existence of the blue phase of dynamical instability (Stothers & Chin 1994, 1996). There seems to be no way out of this dilemma, except to point out one loophole that has so far not been plugged in our models: the possible effect of the acceleration of mass loss on the structure and dynamical stability of the star. This omission we now examine in detail.

4. MASS-LOSS ACCELERATION

The theoretical problem of computing a realistic model for an outflowing stellar envelope has never been wholly solved. Numerical studies of massive stellar models that have treated the coupling of the moving envelope to the deep interior have always had to introduce a number of mathematical simplifications, such as spherical symmetry, steady state flow, and (sometimes) purely radiative transfer of energy (Bisnovatyi-Kogan & Nadyoshin 1972b; Bisnovatyi-Kogan 1973; Zytkow 1973; Turolla, Nobili, & Calvani 1988; Kato & Iben 1992; Schaerer 1996; Heger & Langer 1996). For most upper main-sequence stars, however, this approximate theory seems to work quite well, because the radiation-driven stellar wind is so weak that it produces very little disturbance below the photosphere; therefore, the star's classical position on the H-R diagram is not sensibly affected by the wind (Schaerer et al. 1996).

When the mass-loss rate becomes very high, however, the disturbance of the subphotospheric layers can no longer be disregarded. This is certainly true in the case where the timescale for ejection of the outer envelope is comparable to the envelope's dynamical response time (Zytkow 1972). In this extreme case, the initiation of the outward mass flow must occur inside or even below the iron convection zone, where a huge radiation pressure is created by the iron opacity bump and is accompanied by strong turbulent motions, which become supersonic in the hottest stellar models. Numerical simulation of a representative envelope model with a state-of-the-art hydrodynamical code (L. Dessart 2000, private communication) has recently confirmed the existence of strong convective motions and a rapidly accelerated outward mass flux over one envelope dynamical response time.

How can we describe this perturbation of the subphotospheric layers in an approximate way that is amenable to rapid machine calculation? We recall that the optically thin part of the atmosphere is generally considered to be approximately stationary and governed by a simple, parameterized velocity law. One possibility would be to extend these two assumptions to the underlying layers, all the way down to the sonic point. Another possibility would be to make some equally simple assumption about the time-dependent acceleration in those layers. We have here adopted this second possibility. Accordingly, less attention need be paid to the relatively unimportant problem of the optically thin layers of the atmosphere, which will be treated here in the gray, plane-parallel Eddington approximation, since the interior solution for a radiative envelope always converges quite rapidly to a unique structure below the surface (Schwarzschild 1958; Castor, Abbott, & Klein 1975).

The acceleration of mass loss is far from being a known function, but we may represent it, approximately, as some power law in the radius, $f(r,t) \propto r(t)^b$ under the assumption of spherical symmetry of the outer envelope. This function contains the lifting effect of the steady outward acceleration of material in the outer envelope (analogous to the centrifugal force in the case of rotation). We consider dynamical motions around this steady state flow. The equation of motion for the mass layer $M(r)$ in a nonrotating, nonmagnetic envelope can be written as

$$\frac{d^2r}{dt^2} = -\frac{1}{\rho}\frac{dP}{dr} - g_{\rm eff} \ , \tag{4}$$

where

$$g_{\rm eff} = g - f = g(1-\psi) \tag{5}$$

and $g = GM(r)/r^2$. The ratio f/g is here designated ψ. In general, $P = P_{\rm gas} + P_{\rm rad} + P_{\rm turb}$, but, for simplicity, the turbulent pressure will be ignored as being unimportant in comparison with the gas pressure and radiation pressure. Supplementing equation (4) with the formal definition of the mass density, ρ, in

$$\frac{dM(r)}{dr} = 4\pi r^2 \rho \ , \tag{6}$$

we now perturb all variables in the usual way by writing, for example, $r = r_0 + \delta r \exp(i\sigma t)$, where δr is a small radial displacement. Assuming purely adiabatic perturbations, $\delta P/P_0 = \Gamma_1 \delta\rho/\rho_0$, and linearizing, we eventually find:

$$\frac{d^2}{dr^2}\left(\frac{\delta r}{r}\right) + \left(\frac{4 - V + C}{r}\right)\frac{d}{dr}\left(\frac{\delta r}{r}\right) + \frac{V}{\Gamma_1 r^2}\left[\frac{\sigma^2 r^3}{GM(r)(1-\psi)} - (3\Gamma_1 - 4) + \frac{(2+b)\psi}{1-\psi} + \frac{3\Gamma_1 C}{V}\right]\frac{\delta r}{r} = 0 \ , \tag{7}$$

where $\sigma = 2\pi/\text{period}$, $V = -(d\ln P)/(d\ln r)$, $C = (d\ln\Gamma_1)/(d\ln r)$, and we have dropped the zero subscripts. An eigenvalue σ^2 exists when σ^2 yields $\delta r/r$ finite at the surface and zero at the base of the outer envelope with no nodes lying in between. The necessary and sufficient condition for dynamical instability is, then, that $\sigma^2 \le 0$ (Ledoux 1958; Stothers 1999a).

Notice that equation (7) contains complete generality for any nongravitational force of the form $r(t)^b$. For example, if rotation is considered and if angular momentum is conserved locally, the centrifugal force has an exponent $b = -3$, in which case we recover equation (1) of Stothers (1999b). [A misprint in that equation is corrected here: G should be replaced by $G(1-\lambda)$, where λ is the rotational equivalent of ψ.]

As noted above, the form of the mass-loss acceleration is unknown. In such a state of ignorance it may be safest to assume that f in the outer envelope remains proportional to g at all times, and therefore, in conformity with stationary wind theory (see below), we take $b = -2$. In this case, an approximate solution of equation (7) is

$$\sigma^2 = (5/2)(3\langle\Gamma_1\rangle - 4)(1-\psi)GM/R^3 \ , \tag{8}$$

under the simplifying assumption that the outer envelope has spatially constant values of ρ and $\delta r/r$ (Stothers 1999b). Here $\langle\Gamma_1\rangle$ is the volumetric pressure-weighted mean value of Γ_1. Dynamical instability occurs if $\langle\Gamma_1\rangle \le 4/3$, a condition that is unchanged from the usual criterion without mass loss. Clearly, dynamical instability will also occur if $\psi \ge 1$, but this is a mere formality, since the present formalism breaks down if $\psi \ge 1$ (see below).

We now show how to relate the surface mass-loss rate, dM/dt, to ψ. It is probably a fair approximation to assume the effective gravity, $g_{\rm eff}$, vanishes when the time needed for complete loss of the outer envelope, $\tau_{\rm loss}$, becomes as short as the envelope's dynamical response time, $\tau_{\rm dyn}$. If δM represents the mass of the outer envelope, then

$$\tau_{\rm loss} = \frac{\delta M}{|dM/dt|} \ , \tag{9}$$

while $\tau_{\rm dyn}$ is expected to be some small multiple, h, of the envelope's free-fall collapse time, which can be defined as

$$\tau_{\rm ff} = \left(\frac{R^3}{GM}\right)^{1/2} \ , \tag{10}$$

so that $\tau_{\rm dyn} = h\tau_{\rm ff}$. It is a reasonable assumption to identify $\tau_{\rm dyn}$ as the time required for a sound wave to travel from the surface of the star to the base of the outer envelope and back. Our published numerical hydrodynamical simulations for radiative stellar envelopes that lie either just below or just above the threshold of dynamical stability indicate that $h = 5$–20 (Stothers 1999a). We adopt $h = 10$.

The connecting link between $\tau_{\rm loss}$ and $\tau_{\rm dyn}$ is the effective gravity, $g_{\rm eff}$. Since acceleration goes in general as t^{-2}, elementary dimensional analysis suggests that

$$g_{\rm eff} = \left[1 - \left(\frac{\tau_{\rm dyn}}{\tau_{\rm loss}}\right)^2\right] g \ . \tag{11}$$

This implies $\psi = (\tau_{\rm dyn}/\tau_{\rm loss})^2$. Therefore, the needed relation of ψ to dM/dt is

$$\left|\frac{dM}{dt}\right| = \frac{\psi^{1/2}\delta M}{h\tau_{\rm ff}} \ . \tag{12}$$

Notice that, since $\delta M = (4/3)\pi R^3\langle\rho\rangle$, with $\langle\rho\rangle$ approximately constant, we have $|dM/dt| \propto \psi^{1/2} T_e^{-3} M^{1/2} L^{3/4}$.

It must not be thought that equation (12) imposes an upper limit on the possible rate of mass loss. If the actual rate of mass loss were to exceed the value given by the right-hand side of equation (12) evaluated with $\psi = 1$, this would mean only that more mass than δM gets ejected in a time $\tau_{\rm dyn}$. In such circumstances, the present formalism would break down, and an explicit hydrodynamical calculation of the stellar envelope would be needed. In post–red-supergiant models of LBVs, except for the hottest and brightest objects, ψ remains less than 0.5 (outside of eruption), while in models of comparably bright main-sequence stars ψ is only 10^{-7}, the smallness of this value being due to the large mass contained within the star's outer envelope. On the supposition that η Car is a superluminous main-sequence star (Stothers 2000), ψ outside of eruption would still be only 10^{-2}.

All of the physical uncertainties in the present theoretical formulation are subsumed under the constant parameter h, since we wish to allow ψ to be the one freely adjustable parameter fitted to observations. It is instructive and useful to compare our approach with the traditional stationary wind approach in which the velocity law is typically assumed to be $v(r) = v_\infty(1 - R_0/r)^\beta$, where R_0 and β are adjustable constants and v_∞ is taken from stellar observations. In this formalism, the mass-loss acceleration is given by $f(r) = v\,dv/dr$, a quantity that vanishes at $r = R_0$ (typically taken to be the sonic-point radius) and that behaves like r^{-2} at $r \gg R_0$. Our choice of $b = -2$ is clearly equivalent to considering the regime of supersonic constant flow velocity. By adopting the standard equations of conservation of mass and conservation of momentum (Castor et al. 1975, eqs. [16] and [17]), we can easily make the formal identification:

$$h = \frac{\beta^{1/2}}{3}\left(\frac{R_0}{R}\right)^{1/2}\frac{\langle\rho\rangle}{\rho_R} \ , \tag{13}$$

where ρ_R is the mass density at the photosphere. In the stationary wind approach, $|dM/dt| = 4\pi R^2 \rho_R v_\infty$ and $\psi = v_\infty^2\,\beta R_0/(GM)$, so that the solution is completely determined by the assumed velocity law. In our present approach, we allow ψ to be the adjustable free parameter and link it to dM/dt via equation (12). We can make no prediction for v_∞, which has to be determined from the optically thin layers that are essentially ignored here.

5. GENERALIZED EDDINGTON LUMINOSITY LIMIT

In the outer envelope of the star where the mass $M(r)$ can be taken to be constant, Eddington (1921) showed that the ratio of radiation pressure to total pressure, $1 - \beta$, has a simple analytic expression as long as the material is in radiative, or nearly radiative, equilibrium. In our blue-remnant models, this radiative condition holds to a very close approximation within all layers above the iron convection zone, which forms the base of the outer envelope. Modifying Eddington's relation to allow for a uniform reduction of gravity due to the mass-loss acceleration, we find at any layer r:

$$1 - \beta = \langle\kappa\rangle L/[4\pi c G M(1 - \psi)] \ , \tag{14}$$

where the opacity is averaged with respect to the overlying distribution of radiation pressure:

$$\frac{1}{\langle\kappa\rangle} = \frac{1}{P_{\rm rad}}\int_R^r \frac{1}{\kappa}\frac{dP_{\rm rad}}{dr}dr \ . \tag{15}$$

Equation (14) depends also on the assumption that the luminosity remains essentially unchanged by the work done in lifting matter out of the star's gravitational potential well and in giving the expelled matter its terminal velocity (Forbes 1968; Schaerer 1996; Heger & Langer 1996). This approximation is always valid to within 1% for the blue remnants being considered in this paper if $|dM/dt| < 10^{-4}\ M_\odot\ {\rm yr}^{-1}$.

An upper limit to the star's luminosity can be obtained if we set $\beta = 0$ in equation (14). This condition yields the generalized Eddington luminosity limit,

$$L_{\rm E} = \frac{4\pi c G M(1 - \psi)}{\langle\kappa\rangle} \ . \tag{16}$$

Notice that $L_{\rm E}$ is reduced by the factor $1 - \psi$ from its standard value.

In previous studies of the effects of radiation pressure and the Eddington luminosity limit on blue-remnant models, attention was focused on the driving efficiency of atomic line opacity. Although only the hydrogen-free Wolf-Rayet stars were modeled in those studies, the results obtained are of more general applicability because LBVs, like Wolf-Rayet stars, possess high central condensations, small-mass outer envelopes, and large surface radii caused by the iron opacity bump. A dispute still exists about whether metallic absorption lines above the photosphere can provide all of the momentum needed to drive the large observed mass-loss fluxes of 10^{-5} to $10^{-4}\ M_\odot\ {\rm yr}^{-1}$ (Pauldrach et al. 1985; Turolla et al. 1988; Lucy & Abbott 1993; Pistinner & Eichler 1995; Schmutz 1997) or whether the iron opacity bump is indispensable in getting the mass-loss process started inside the optically thick layers below the photosphere (Kato & Iben 1992; Eichler, Bar Shalom, & Oreg 1995). A potential problem is that convective motions in the iron convection zone may carry a significant portion of the total flux coming from the undisturbed interior, making it less likely that a super-Eddington radiative luminosity below the photosphere can successfully accelerate matter outward (Schaerer 1996). Although strange-mode pulsations (Heger & Langer 1996) or convective turbulence (Stothers 2000) might provide the missing momentum for the surface mass loss, our new models suggest that the iron convection zone in the hottest of the blue remnants actually becomes radiatively unstable by itself, owing to the fact that the mass-loss acceleration and high opacities bring the Eddington limit down far enough.

6. MODIFIED STELLAR EVOLUTIONARY MODELS

In order to incorporate the mass-loss acceleration in our stellar models, we shall adopt the hydrostatic version of equation (4) with a modified gravity and the linear adiabatic wave equation (7) with $b = -2$. For simplicity, we assume that ψ is constant with depth in the outer envelope.

The formal limiting case is represented by $\psi = 1$. In practice, this limit cannot be reached because the Eddington limit, at which $\beta = 0$ and so $\rho = 0$, will be reached first. If $L \geq L_{\rm E}$ locally, and if convection is absent or inefficient, the overlying layers will be expelled by radiation pressure. In our models, this radiative instability occurs for values of ψ that are sufficiently large but still less than unity. The layers in which the local mass density, ρ, formally vanishes always lie inside the iron convection zone owing to the large opacities there.

Recomputation of our outer envelope models to include the mass-loss acceleration can be done without recalculating any of the evolutionary tracks, since the stellar interior is unaffected and the structure of the outer envelope is simply determined by performing a numerical integration down from the surface, after specifying the envelope parameters M, $X_{\rm surf}$, Z_e, α_P, L, T_e, and ψ. The needed luminosities for fixed M, $X_{\rm surf}$, Z_e, and α_P are taken from § 3. The effective temperatures, however, must be recomputed, and it is also necessary to determine ψ. This is done by computing a large set of envelope models for various ψ and T_e values, and by finding that particular model which attains *simultaneously* the thresholds of radiative instability and of dynamical instability, because each threshold can determine only one free parameter, ψ or T_e. Although we cannot prove uniqueness of our solution rigorously, we have never found an actual counterexample in practice.

Table 3 contains our derived values of ψ and T_e for 10 representative stellar models, which include four blue-remnant masses and three evolutionary stages. In the case of the smallest mass, only one stage appears, because dynamical instability for this mass does not occur until the end of central helium burning.

Examination of Table 3 leads to several interesting conclusions about the critical effective temperature for such a double instability. First, T_e turns out to be virtually independent of the stellar mass, luminosity, and surface hydrogen abundance—in other words, of all of the present evolutionary uncertainties about the blue remnants. Second, T_e represents the highest value possible for a blue remnant at the threshold of dynamical instability, because hotter models are found to be only radiatively (and not dynamically) unstable if other parameters are held fixed. Third, T_e shows only a weak dependence on the convective mixing length, increasing from 22,000 K for $\alpha_P = 1.4$ to 29,000 K for $\alpha_P = 2.8$. Under the assumption of even larger values of α_P, little further increase of T_e could be gained, since for an effective temperature above ~30,000 K hydrogen and helium are completely ionized and dynamical instability is then not possible in any case.

The reason why the critical effective temperature increases with α_P is easy to understand. Models with more efficient convection (greater α_P) allow a larger luminous flux to be transported without disruption to the envelope. Therefore, a larger ψ can be tolerated, augmenting the relative pressure of radiation. This lowers $\langle \Gamma_1 \rangle$ and so increases the envelope's tendency to dynamical instability. Consequently, dynamical instability can occur at a higher effective temperature, where, otherwise, the zones of partial ionization of hydrogen and helium would be too small to be of much importance.

Mass-loss rates at the critical effective temperature can be computed from equation (12). These are also entered in Table 3. If the observed mass-loss rate at any critical effective temperature were to exceed the listed value, the outer envelope would be radiatively unstable. It is, therefore, reassuring to note how similar the critical mass-loss rates found here are to those derived previously for Wolf-Rayet model envelopes by using traditional stationary wind theory (Kato & Iben 1992; Schaerer 1996; Heger & Langer 1996).

If, on the other hand, the observed mass-loss rate were found to be less than the critical value listed in Table 3, the outer envelope would be radiatively stable. We now consider such radiatively stable envelope models. By formally assigning a (subcritical) mass-loss rate, the two quantities ψ and T_e can be uniquely determined so as to satisfy the condition that the model lie exactly at the threshold of dynamical instability. Because $|dM/dt| \propto \psi^{1/2} T_e^{-3}$, approximately, and the dependence of T_e on ψ is very weak at the threshold, the critical effective temperature will formally decrease if the mass-loss rate is increased. Derived T_e values are presented in Table 4 for $\alpha_P = 1.4$ and in Table 5 for $\alpha_P = 2.8$. The tabulated mass-loss rates run from $\log |\dot{M}| = -4.4$ down to

TABLE 3

THRESHOLD OF DYNAMICAL INSTABILITY FOR MODIFIED HOT MODELS AT THE EDDINGTON LIMIT

				$\alpha_P = 1.4$			$\alpha_P = 2.8$		
REMNANT $M/M_\odot$	$X_{\rm surf}$	$\log (L/L_\odot)$	Y_c	ψ	$\log T_e$	$\log \lvert\dot{M}\rvert$	ψ	$\log T_e$	$\log \lvert\dot{M}\rvert$
10.4	0.22	5.474	0.003	0.15	4.36	−4.89	0.24	4.47	−5.57
15.4	0.39	5.479	0.95	0.36	4.31	−4.67	0.42	4.45	−5.34
		5.572	0.19	0.23	4.33	−4.82	0.30	4.45	−5.43
		5.657	0.003	0.07	4.32	−5.00	0.16	4.45	−5.53
21.6	0.27	5.733	0.95	0.27	4.35	−4.55	0.34	4.46	−5.21
		5.802	0.24	0.16	4.35	−4.67	0.24	4.46	−5.30
		5.880	0.003	0.01	4.36	−5.28	0.10	4.46	−5.46
34.6	0.24	6.052	0.95	0.11	4.35	−4.53	0.20	4.45	−5.13
		6.113	0.20	0.00	[a]	[a]	0.09	4.45	−5.29
		6.170	0.003	0.00	[a]	[a]	0.00	[a]	[a]

[a] Models at all effective temperatures are either dynamically unstable or radiatively unstable.

TABLE 4
THRESHOLD OF DYNAMICAL INSTABILITY FOR MODIFIED HOT MODELS IN THE CASE $\alpha_P = 1.4$

				$\log T_e$	
REMNANT $M/M_\odot$	$X_{\rm surf}$	$\log (L/L_\odot)$	Y_c	$\log \lvert\dot{M}\rvert = -4.4$	$\log \lvert\dot{M}\rvert = -4.7$
10.4	0.22	5.474	0.003	4.20	4.31
15.4	0.39	5.479	0.95	4.23	4.31
		5.572	0.19	4.21	4.30
		5.657	0.003	[a]	[a]
21.6	0.27	5.733	0.95	4.31	4.35
		5.802	0.24	4.28	4.35
		5.880	0.003	[a]	[a]
34.6	0.24	6.052	0.95	4.31	4.35
		6.113	0.20	[a]	[a]
		6.170	0.003	[a]	[a]

[a] Models at all effective temperatures are either dynamically unstable or radiatively unstable.

the corresponding limits already listed in Table 3, in steps of -0.3. The dependence of the results on α_P is slight, as expected.

Stellar models at the threshold of dynamical instability are plotted on the H-R diagram in Figure 2 for $\alpha_P = 1.4$ and in Figure 3 for $\alpha_P = 2.8$. Separate loci are shown for each of the blue-remnant masses and for each specified mass-loss rate. To the left of each plotted locus, progressively hotter stellar models with the same mass-loss rate become progressively more dynamically unstable until radiative instability also sets in. The threshold effective temperature for radiative instability may in some cases lie beyond the ionization limit for dynamical instability, ~30,000 K. To the right of each plotted locus, cooler stellar models with the same mass-loss rate become progressively more stable dynamically until they cross the threshold of dynamical instability just to the left of the threshold that exists in the formal absence of mass loss (Fig. 1).

To compare these predictions with observations, nine LBVs and LBV candidates whose mass-loss rates have been measured at times of quiescence are plotted in Figures 2 and 3 (the nine stars are identified in Table 6). It is clear that the three least luminous objects have mass-loss rates that are small enough as not to interfere with the determination of their dynamical stability or instability. Our earlier conclusion (based on Fig. 1) that these three objects are probably encountering dynamical instability remains unchanged.

As for the six brighter LBVs, two of the three faintest in this group show mass-loss rates that agree closely with our revised predictions for blue remnants at the threshold of dynamical instability. The one exception is *R* 71, having $\log \lvert\dot{M}\rvert = -6.2$ according to Leitherer (1997), for which we would have expected to find $\log \lvert\dot{M}\rvert = -4.7$. This star's mass-loss rate should perhaps be remeasured in view of the fact that Leitherer (1997) originally estimated $\log \lvert\dot{M}\rvert = -6.15$ for HR Car, whereas later work (White 2000) increased this to -4.7.

The three brightest LBVs that are plotted show mass-loss rates so large that their outer envelopes must be radiatively unstable, according to our revised stellar models. Their atmospheres must be radiatively unstable, too (de Jager et al. 2001). Notice that the measured rates lie an order of magnitude above those of ordinary O and B supergiants with the same luminosities (Scuderi et al. 1998). This alone would suggest that these three stars are not main-sequence objects.

7. CONCLUSION

An extensive parameter study has been conducted in order to understand better the observed properties of LBVs,

TABLE 5
THRESHOLD OF DYNAMICAL INSTABILITY FOR MODIFIED HOT MODELS IN THE CASE $\alpha_P = 2.8$

				$\log T_e$			
REMNANT $M/M_\odot$	$X_{\rm surf}$	$\log (L/L_\odot)$	Y_c	$\log \lvert\dot{M}\rvert = -4.4$	$\log \lvert\dot{M}\rvert = -4.7$	$\log \lvert\dot{M}\rvert = -5.0$	$\log \lvert\dot{M}\rvert = -5.3$
10.4	0.22	5.474	0.003	4.19	4.28	4.37	4.44
15.4	0.39	5.479	0.95	4.20	4.29	4.38	4.44
		5.572	0.19	4.18	4.27	4.36	4.43
		5.657	0.003	4.05	4.20	4.31	4.40
21.6	0.27	5.733	0.95	4.28	4.36	4.42	4.46
		5.802	0.24	4.25	4.34	4.41	4.46
		5.880	0.003	[a]	[a]	4.33	4.42
34.6	0.24	6.052	0.95	4.29	4.37	4.43	4.45
		6.113	0.20	[a]	[a]	4.38	4.45
		6.170	0.003	[a]	[a]	[a]	[a]

[a] Models at all effective temperatures are either dynamically unstable or radiatively unstable.

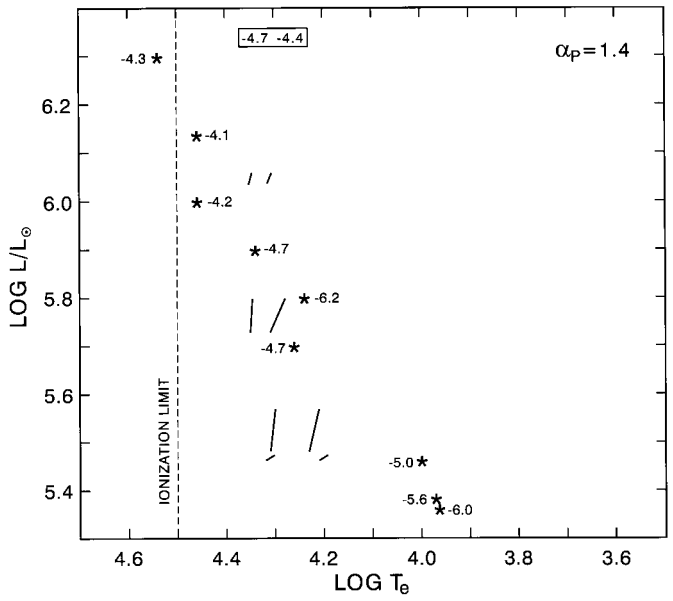

FIG. 2.—H-R diagram showing the possible locations of stellar models at the threshold of dynamical instability, for four blue-remnant masses in the case $\alpha_P = 1.4$. All models include the effect of the mass-loss acceleration, for which the associated values of $\log|\dot{M}|$ are indicated in the rectangular box at the top. To the left of the plotted loci lies the domain of dynamical (and radiative) instability for each associated mass-loss rate, although dynamical instability itself cannot occur blueward of the dashed line representing the ionization limit. Asterisks denote well-observed LBVs and LBV candidates at quiescence whose mass-loss rates are known. Observed values of $\log|\dot{M}|$ are indicated.

here considered to be post–red-supergiant stars. Input parameters that have been freely varied in the present work include the following: surface mass-loss rates for main-sequence stars, for red supergiants, and for blue remnants; mass of the helium core in the blue remnant; mass of the hydrogen envelope; central helium abundance, Y_c; $^{12}C(\alpha,\gamma)^{16}O$ reaction rate; convective core overshooting distance; axial rotation rate; envelope metal opacities; convective envelope mixing-length parameter, α_P; and ratio of mass-loss acceleration to gravitational acceleration, ψ. Of these, the most influential factors are the helium core mass, the hydrogen envelope mass, Y_c, and ψ. The helium core mass establishes the luminosity of the blue remnant, while the three other parameters mainly regulate its effective temperature, primarily through their fine-tuning of the Eddington luminosity ratio L_E/L. Linkage of ψ to the actual mass-loss rate occurs via equation (12).

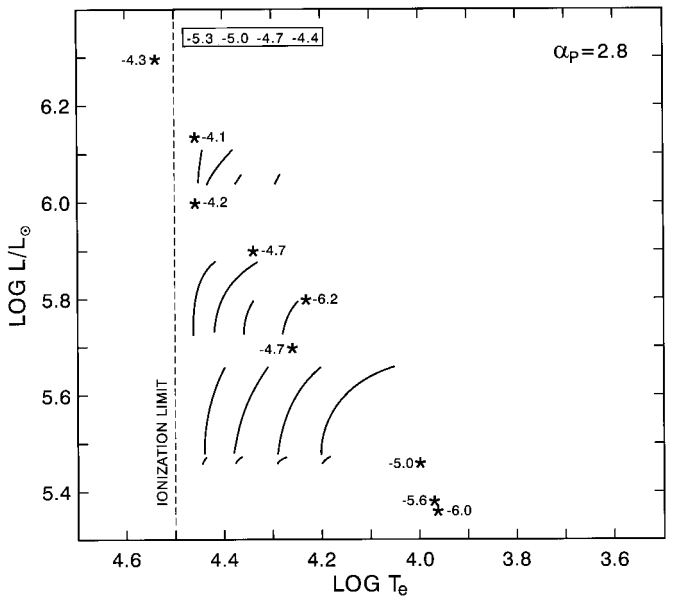

FIG. 3.—Same as Fig. 2, but for $\alpha_P = 2.8$

A consistent evolutionary picture of the LBVs can now be sketched. Except for the very rare superluminous objects like η Car, classical LBVs have most likely originated from massive late-type helium-burning supergiants, probably in a yellow-red phase of dynamical instability (Stothers & Chin 1996). In all cases, their lifetimes are a small fraction of the star's total helium-burning lifetime of $(2–3) \times 10^5$ yr. We now discuss these stars in more detail after grouping them into three ranges of luminosity.

Faint LBVs with $\log(L/L_\odot) = 5.4–5.7$.—Stars with these luminosities emerge from the red-supergiant region as dynamically unstable yellow supergiants, and then execute a wide blue loop on the H-R diagram. When they cool to 10,000–15,000 K, dynamical instability sets in for the second time. Figure 1 confirms that predicted and observed effective temperatures for such faint, cool LBVs agree with each other. Theoretical lifetimes range from $\sim 10^3$ yr at $\log(L/L_\odot) = 5.4$ (Stothers & Chin 1996) to $\sim 2 \times 10^4$ yr at $\log(L/L_\odot) = 5.7$ (see below); the average value is perhaps $\sim 1 \times 10^4$ yr. Transient blue loops are repeatedly triggered by the dynamical instability (Stothers & Chin 1995). If either the original blue loop or any of the transient blue loops extends past ~30,000 K, the star could become radiatively unstable at that time, provided that its accompanying mass-loss rate is equal to or greater than what is now observed in its LBV state, specifically, $\log|\dot{M}| \geq -5.5$. We note that such hot objects could appear as hydrogen-poor WN stars. Observed WN stars of the appropriate luminosity and effective temperature show, in fact, $\log|\dot{M}| \approx -4.7$ (Nugis & Niedzielski 1995; Leitherer, Chapman, & Koribalski 1997; Hamann & Koesterke 1998a, 1998b, 2000; Nugis, Crowther, & Willis 1998).

Intermediate-luminosity LBVs with $\log(L/L_\odot) = 5.7–6.0$.—The post–red-supergiant phase begins with a dynamically unstable yellow-supergiant phase, followed by a long blue loop. Near the tip of the loop, the blue remnant encounters radiative instability. Evolving away from the tip as helium is further depleted, the star eventually becomes dynamically unstable (for the second time) at effective temperatures of 20,000–30,000 K if, as is observed, $\log|\dot{M}| \approx -4.7$. (The effect of the mass-loss acceleration raising the threshold effective temperature from ~12,000 K is very substantial.) Mass loss occurs heavily from now on in repeated cycles until hydrogen is completely gone from the star. Meanwhile, the star's evolution stalls in this general region of the H-R diagram owing to its continuing, rapid loss of hydrogen and the resulting short lifetime of this phase, $\sim 5 \times 10^4$ yr, of which the final $\sim 3 \times 10^4$ yr (or more) are spent in the hydrogen-poor WN state (Stothers & Chin 2000).

Bright LBVs with $\log(L/L_\odot) = 6.0–6.3$.—These stars may never have been red at all, although they are expected to have briefly occupied the yellow region, when they would have been dynamically unstable for a short time. They are now very blue. Radiative instability (and dynamical insta-

TABLE 6
OBSERVED LBVs AND LBV CANDIDATES WITH KNOWN MASS-LOSS RATES AT QUIESCENCE

Variable	Galaxy	$\log(L/L_\odot)$	$\log T_e$	$\log\lvert\dot{M}\rvert$	References
S Dor	LMC	6.30	4.54	−4.3	1, 2
AG Car	MW	6.14	4.46	−4.1	1, 2
R127	LMC	6.00	4.46	−4.2	1, 2
HR Car	MW	5.90	4.34	−4.7	1, 3
R71	LMC	5.80	4.24	−6.2	1, 2
P Cyg	MW	5.70	4.26	−4.7	1, 2
HD 160529...	MW	5.46	4.00	−5.0	1, 2
HD 168607...	MW	5.38	3.97	−5.6	1, 4
R110	LMC	5.36	3.96	−6.0	1, 2

REFERENCES.—(1) van Genderen 2001; (2) Leitherer 1997; (3) White 2000; (4) Leitherer, Chapman, & Koribalski 1995.

bility, too, if $T_e < 30{,}000$ K) theoretically persists from this time onward, because at the observed mass-loss rate of $\log|\dot{M}| = -4.2$ the residual hydrogen envelope is stripped off in a mere $\sim 1 \times 10^4$ yr. Such a bright and hot LBV is expected to look like a hydrogen-poor WN star, which some observations apparently confirm (Pasquali et al. 1997). Although observations also support our theoretically predicted effective temperatures of 20,000–30,000 K, the apparent agreement may be somewhat misleading. Observationally, it is uncertain whether the true photospheres of these heavily mass-losing stars have been observed or not (de Koter, Lamers, & Schmutz 1996). Theoretically, the effective temperatures of our models are also unreliable for mass-loss rates that are so large that they perturb the star's structure to depths lying well below the iron convection zone.

The chief lack now in our evolutionary models is a hydrodynamical computation of the turbulent outer envelope. There seems to be no acceptable way to substitute a static boundary condition or even a stationary-flow atmospheric model as a boundary condition if the mass-loss rate exceeds $\log|\dot{M}| = -4.7$. In stars so luminous and hot, the entire outer envelope (and perhaps even some of the deeper layers) must be treated as representing the massive outflowing stellar wind.

It is a great pleasure to acknowledge many helpful communications from C.-w. Chin, L. Dessart, A. M. van Genderen, and C. de Jager. The referee's detailed suggestions for improvements of the text are also much appreciated. This work was supported in part by the NASA Climate Research Program.

REFERENCES

Baumgarte, T. W., & Shapiro, S. L. 1999, ApJ, 526, 937
Bisnovatyi-Kogan, G. S. 1973, Ap&SS, 22, 307
Bisnovatyi-Kogan, G. S., & Nadyoshin, D. K. 1972, Ap&SS, 15, 353
Castor, J. I., Abbott, D. C., & Klein, R. I. 1975, ApJ, 195, 157
Cox, J. P., & Salpeter, E. E. 1961, ApJ, 133, 764
de Jager, C. 1998, A&AR, 8, 145
de Jager, C., Lobel, A., Nieuwenhuijzen, H., & Stothers, R. 2001, MNRAS, 327, 452
de Koter, A., Lamers, H. J. G. L. M., & Schmutz, W. 1996, A&A, 306, 501
Eddington, A. S. 1921, Z. Phys., 7, 351
Eichler, D., Bar Shalom, A., & Oreg, J. 1995, ApJ, 448, 858
Endal, A. S., & Sofia, S. 1978, ApJ, 220, 279
Forbes, J. E. 1968, ApJ, 153, 495
Giannone, P. 1967, Z. Astrophys., 65, 226
Glatzel, W. 1998, A&A, 339, L5
Hamann, W.-R., & Koesterke, L. 1998a, A&A, 333, 251
———. 1998b, A&A, 335, 1003
———. 2000, A&A, 360, 647
Heger, A., & Langer, N. 1996, A&A, 315, 421
———. 1998, A&A, 334, 210
Humphreys, R. M., & Davidson, K. 1979, ApJ, 232, 409
———. 1994, PASP, 106, 1025
Humphreys, R. M., et al. 1997, AJ, 114, 2778
Iglesias, C. A., & Rogers, F. J. 1996, ApJ, 464, 943
Iglesias, C. A., Rogers F. J., & Wilson, B. G. 1992, ApJ, 397, 717
Josselin, E., Blommaert, J. A. D. L., Groenewegen, M. A. T., Omont, A., & Li, F. L. 2000, A&A, 357, 225
Kato, M., & Iben, I., Jr. 1992, ApJ, 394, 305
Lamers, H. J. G. L. M., de Groot, M., & Cassatella, A. 1983, A&A, 123, L8
Lamers, H. J. G. L. M., Haser, S., de Koter, A., & Leitherer, C. 1999, ApJ, 516, 872
Lamers, H. J. G. L. M., Nota, A., Panagia, N., Smith, L. J., & Langer, N. 2001, ApJ, 551, 764
Langer, N. 1987, A&A, 171, L1
———. 1997, in ASP Conf. Ser. 120, Luminous Blue Variables: Massive Stars in Transition, ed. A. Nota & H. J. G. L. M. Lamers (San Francisco: ASP), 83
Langer, N., Hamann, W.-R., Lennon, M., Najarro, F., Pauldrach, A. W. A., & Puls, J. 1994, A&A, 290, 819
Ledoux, P. 1958, in Handbuch der Physik, Vol. 51, ed. S. Flügge (Berlin: Springer), 605
Leitherer, C. 1997, in ASP Conf. Ser. 120, Luminous Blue Variables: Massive Stars in Transition, ed. A. Nota & H. J. G. L. M. Lamers (San Francisco: ASP), 58
Leitherer, C., Chapman, J. M., & Koribalski, B. 1995, ApJ, 450, 289
———. 1997, ApJ, 481, 898
Lucy, L. B., & Abbott, D. C. 1993, ApJ, 405, 738
Maeder, A. 1999, A&A, 347, 185
Maeder, A., & Meynet, G. 2000a, ARA&A, 38, 143
———. 2000b, A&A, 361, 159
Meaburn, J., O'Connor, J. A., López, J. A., Bryce, M., Redman, M. P., & Noriega-Crespo, A. 2000, MNRAS, 318, 561
Meynet, G., Maeder, A., Schaller, G., Schaerer, D., & Charbonnel, C. 1994, A&AS, 103, 97
Nedoluha, G. E., & Bowers, P. F. 1992, ApJ, 392, 249
Nieuwenhuijzen, H., & de Jager, C. 1990, A&A, 231, 134
Nugis, T., Crowther, P. A., & Willis, A. J. 1998, A&A, 333, 956
Nugis, T., & Niedzielski, A. 1995, A&A, 300, 237
Oudmaijer, R. D., Groenewegen, M. A. T., Matthews, H. E., Blommaert, J. A. D. L., & Sahu, K. C. 1996, MNRAS, 280, 1062
Pasquali, A., Langer, N., Schmutz, W., Leitherer, C., Nota, A., Hubeny, I., & Moffat, A. F. J. 1997, ApJ, 478, 340
Pauldrach, A. W. A., & Puls, J. 1990, A&A, 237, 409
Pauldrach, A. W. A., Puls, J., Hummer, D. G., & Kudritzki, R. P. 1985, A&A, 148, L1
Pistinner, S., & Eichler, D. 1995, ApJ, 454, 404
Robberto, M., Ferrari, A., Nota, A., & Paresce, F. 1993, A&A, 269, 330
Rogers, F. J., & Iglesias, C. A. 1992, ApJS, 79, 507
Sackmann, I. J., & Anand, S. P. S. 1970, ApJ, 162, 105
Salasnich, B., Bressan, A., & Chiosi, C. 1999, A&A, 342, 131
Schaerer, D. 1996, A&A, 310, 129
Schaerer, D., de Koter, A., Schmutz, W., & Maeder, A. 1996, A&A, 310, 837
Schaller, G., Schaerer, D., Meynet, G., & Maeder, A. 1992, A&AS, 96, 269
Schmutz, W. 1997, A&A, 321, 268
Schwarzschild, M. 1958, Structure and Evolution of the Stars (Princeton: Princeton Univ. Press)

Scuderi, S., Panagia, N., Stanghellini, C., Trigilio, C., & Umana, G. 1998, A&A, 332, 251
Seaton, M. J., Yan, Y., Mihalas, D., & Pradhan, A. K. 1994, MNRAS, 266, 805
Simon, N. R., & Stothers, R. B. 1969, ApJ, 155, 247
Smith, L. J., Nota, A., Pasquali, A., Leitherer, C., Clampin, M., & Crowther, P. A. 1998, ApJ, 503, 278
Smith, L. J., Stroud, M., Esteban, C., & Vilchez, J. M. 1997, MNRAS, 290, 265
Staritsin, E. I., & Tutukov, A. V. 1989, Soviet Astron., 33, 144
Sterken, C., de Groot, M., & van Genderen, A. M. 1997, A&A, 326, 640
Stothers, R. B. 1999a, MNRAS, 305, 365
———. 1999b, ApJ, 513, 460
———. 1999c, ApJ, 516, 366
———. 2000, ApJ, 530, L103
Stothers, R. B., & Chin, C.-w. 1976, ApJ, 204, 472
———. 1994, ApJ, 426, L43
———. 1995, ApJ, 451, L61
———. 1996, ApJ, 468, 842
———. 1997, ApJ, 478, L103
———. 1999, ApJ, 522, 960
———. 2000, ApJ, 540, 1041
Turolla, R., Nobili, L., & Calvani, M. 1988, ApJ, 324, 899
van Genderen, A. M. 2001, A&A, 366, 508
Voors, R. H. M., et al. 2000, A&A, 356, 501
White, S. M. 2000, ApJ, 539, 851
Wittkowski, M., Langer, N., & Weigelt, G. 1998, A&A, 340, L39
Zytkow, A., 1972, Acta Astron., 22, 103
———. 1973, Acta Astron., 23, 121